Journal of Constructional Steel Research 203 (2023) 107832

Contents lists available at ScienceDirect

Journal of Constructional Steel Research

journal homepage: www.elsevier.com/locate/jcsr

Effects of reinforcing steel tanks with intermediate ring stiffeners on wind buckling during construction

Özer Zeybek [a], Yasin Onuralp Özkılıç [b,*]

[a] Department of Civil Engineering, Mugla Sitki Kocman University, Mugla 48000, Turkey
[b] Department of Civil Engineering, Necmettin Erbakan University, Konya, 42090, Turkey

ARTICLE INFO

Keywords:
Cylindrical storage tank
Construction stage
IRS
Collapse
Buckling
Imperfection sensitivity

ABSTRACT

Many tank structures may not be stable during the construction phase, and this may lead to their becoming vulnerable to buckling under environmental loading conditions such as wind. Installing intermediate ring stiffeners of the proper size at the mid-height of the cylindrical shell may be the most effective way to stabilize these structures, especially under the effects of wind action. In the study, analytical and numerical studies were conducted to identify the required strength and stiffness for the intermediate ring stiffener. First, a new cylindrical shell-to- intermediate ring stiffness ratio was derived by considering curved beam and shell membrane theories. For strength criteria, the tributary height and the effect of shell- ring interaction on the internal forces and moments were examined by making use of Linear Analysis (LA) and Geometrically Nonlinear Analysis (GNA). The stress resultants developed in the intermediate ring stiffener were identified so that they could be used as strength criteria. For stiffness criteria, by considering the changes in the buckling resistance based on the developed stiffness ratio, an expression to compute the minumum intermediate ring stiffness was determined. In addition, Geometrically Nonlinear Analysis including Imperfections (GNIA) was also performed to examine the effect of the geometric imperfections on buckling strength of the steel tank with an intermediate ring stiffener, taking different imperfection amplitudes into account. The developed design equations in simple algebraic form can be utilized for the structural stability of cylindrical steel tanks during erection.

1. Introduction

Cylindrical steel tanks are often used for the storage of liquids such as chemicals, water and oil. In these types of cylindrical structures, curved thin steel plates are used to form shell courses. Using welds, the courses are mounted on top of each other to form the entire tank shell wall. After this is done, a roof is placed on the top of the tanks to provide stability. However, evidence from failures in many tank structures reveals that, before the installation of the roofs, the tanks themselves suffer buckling due to external pressure, since the thin walls are vulnarable to buckling. In other words, since they do not resist environmental loading conditions such as wind before completion, unexpected failure may be observed in such storage tank structures [1]. As shown in Fig. 1, while TK-7 and TK-8 were subjected to high damage, other tank structures suffered minor or no damage due to supporting members such as rafter and roof at the top. Saal and Schrüfer [2] investigated tanks without roof structures, which is the situation before the construction is complete. Researchers examined the stability behaviour of these types of tanks. Ansourion [3] reported that inadequate top restraint during construction led to failure of the tank which was exposed to wind loads. Noon [4] stated that relatively moderate wind led to failure of a storage tank due to lack of bracing before the construction was complete. A specific tank failure during the erection stage was shown in the study. Borgersen and Yazdani [5] examined large scale storage tanks during erection under wind pressure. The cylindrical shell (CS) part had been completed, but the conical roof had not been attached to the top of the tank when buckling was observed at a wind speed of 100 km/h. Considering FE analyses, the failure mode was also identified in the study. Jaca and Godoy [6] reported that many tank structures in Argentina collapsed during their construction stages due to wind loads. Although storage tanks were designed considering complete structures such as the foundation, cylindrical part and roof, they failed due to moderate wind before the roof was added to the top of the structure.

The abovementioned studies revealed that such storage tanks are flexible during the construction stage even if they are designed carefully considering all loads. Normally, wind stiffeners are designed to prevent

* Corresponding author.
E-mail address: yozkilic@erbakan.edu.tr (Y.O. Özkılıç).

https://doi.org/10.1016/j.jcsr.2023.107832
Received 12 July 2022; Received in revised form 19 January 2023; Accepted 23 January 2023
Available online 3 February 2023

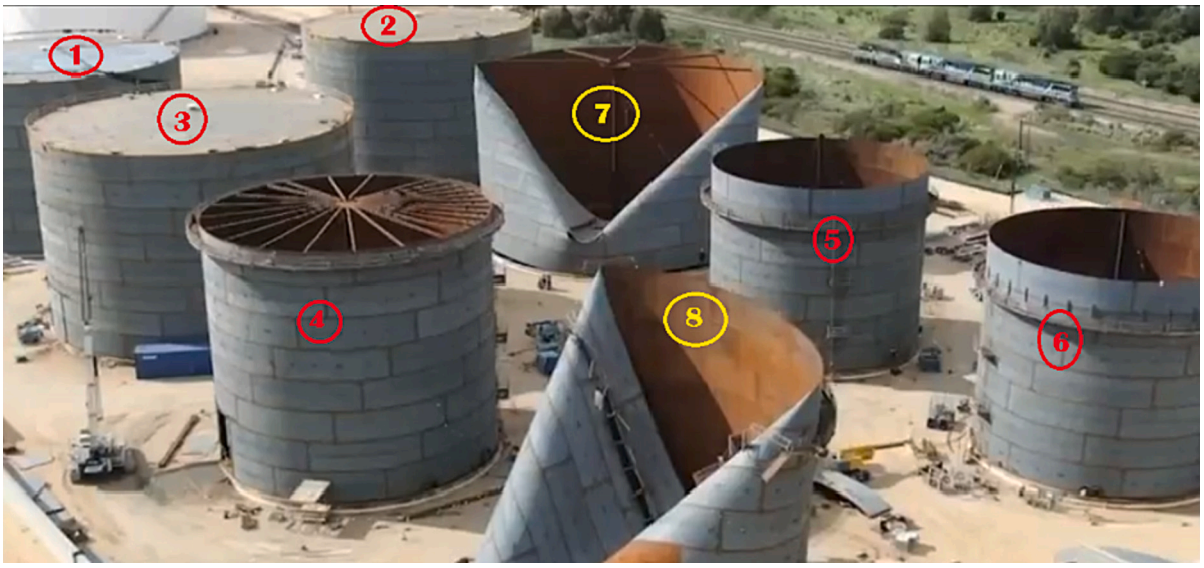

Fig. 1. Example of tank failures during construction stage (Courtesy of Mr. Oscar Enrique Morillo Luzardo).

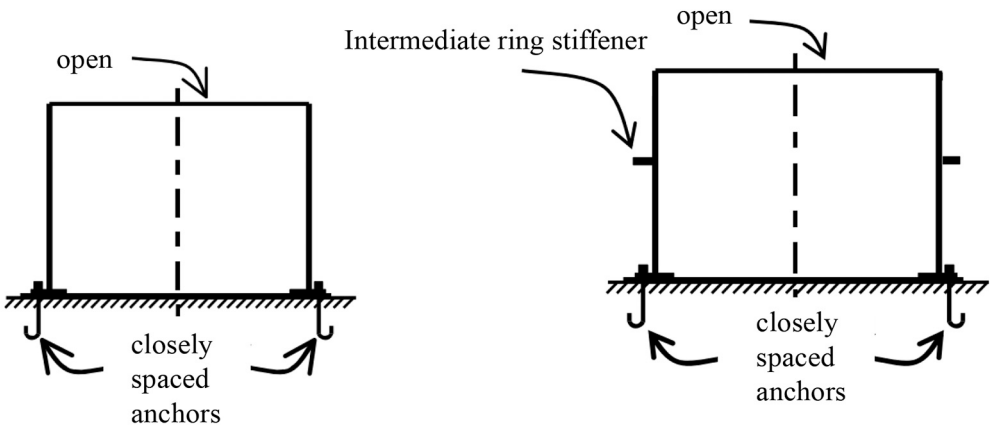

a) a cylindrical shell with an unrestrained upper-edge (before a fixed roof is installed) b) a cylindrical shell with an intermediate ring stiffener

Fig. 2. Different cylindrical shell configurations (Adapted from [52]).

wind buckling, considering that the tank structures are already in service. However, a tank structure during its construction is weak and susceptible to possible failure. It has also been noted that wind pressure varies widely throughout the day. There is no design guideline foreseeing such tank failures during the erection stage. From this motivation, the weakness of the shell part of the structures was addressed and the effect of reinforcing steel tanks with stiffeners on buckling due to wind has been investigated in this new study. One of the common ways to increase the load carrying capacity of these structures is to use intermediate ring stiffeners (IRS) at mid-height when they are subjected to environmental loads such as wind. IRS have an important job, which is to provide the safe and reliable operation of tanks [7]. Furthermore, IRS should sustain roundness on the CS under different loading circumstances [8]. In this way, IRS stabilize the full tank height before the roof is attached. In other words, the buckling capacity of the CS can be enhanced significantly when compared with the CS without any stiffener (Fig. 2a). To investigate the effect of the inclusion of the intermediate ring stiffener (IRS) on the load carrying capacity for these structures, an approach needs to satisfy both the strength and stiffness requirements for cylindrical steel tanks. As shown in Fig. 2b, a single IRS is installed at mid-height of the CS before the completion of the roof part. This ring provides higher stability for the thin cylindrical storage tank which is vulnerable to buckling when exposed to wind. Analytical and numerical studies were combined to achieve stable behaviour of these structures when they are subjected to wind pressure during the construction stage. In the first stage, the required strength of the ring was identified by making use of a closed-form solution and complementary finite element analysis. For this purpose, the behaviour of an IRS and CS under non uniform wind loading was studied separately. Next, a cylindrical shell-to- ring (CS-to- IRS) stiffness ratio was proposed to reflect the interaction between the ring and shell. Moreover, the tank tributary height (h_{eff}) was determined as a function of the CS-to- IRS stiffness ratio. Parametric calculations including Linear Analysis (LA) were performed to develop a relationship between the proposed CS-to-IRS stiffness ratio and the responses of the ring computed from the closed-form solutions. Additionally, the effect of geometric nonlinearity on the responses of the

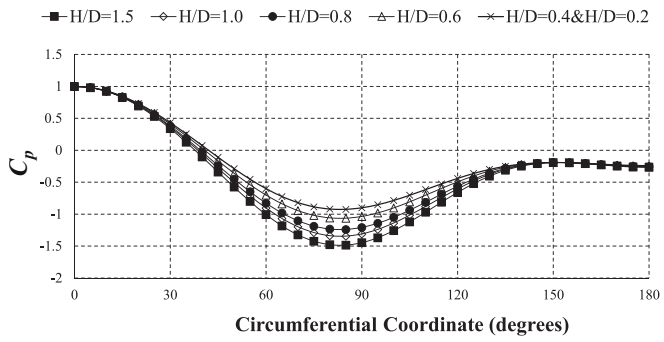

a) for closed roof

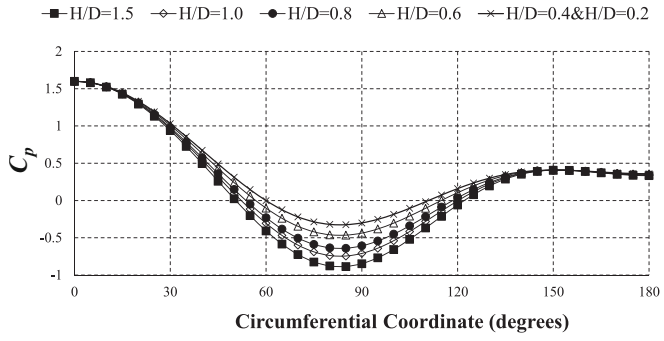

b) for open top

Fig. 3. Distribution of wind pressure around circumference ([37]).

2. Wind pressures on cylindrical shell structures

Wind loading and internal partial vacuums are common external pressures that can cause the failure of tank structures. In other words, since the CS has quite thin walls, it is vulnerable to buckling under external pressure. Furthermore, this is aggravated under wind loading because the wind pressure is changing importantly along the circumferential direction, causing local flattening of the wall and inducing stresses in different directions [11–14]. Hence, the variation of wind pressure around the circumference may be crucial in design.

The effect of wind loading on cylindrical structures was investigated utilizing wind tunnel tests [11,15–25]. The outcomes revealed that the wind load changes with the circumferential directions of the cylinder. Nevertheless, the wind load in the vertical direction is generally taken as constant [26–31] because the aspect ratio of CS is relatively small. Depending on the size of the CS, wind loads in circumferential direction (Fig. 3) can be computed by a Fourier harmonic cosine series [32–39]. Eq. (1) describes the principal wind profile along the circumferential direction.

$$q_w(\theta) = \sum_{m=0}^{N} q\, C_m cos(m\theta) \tag{1}$$

where $q_w(\theta)$ = the local wind pressure at any point on the circumference, q = the wind pressure on the stagnation meridian, θ = the circumferential angle measured from the windward direction ($\theta = 0$ at the stagnation meridian), m = the harmonic number, C_m = coefficient for each harmonic and N = the total number of harmonics being considered.

A representation of the distrubition of the wind pressure for open-top and closed roof CS is illustrated in Fig. 3 with the values of C_m. The coefficients are given in Annex C of EN 1993-4-1 [37] as follows:

$$C_{p,e}(\theta) = C_m cos(m\theta) = -0.54 + 0.16(D/H) + \{0.28 + 0.04(D/H)\}cos\theta + \{1.04 - 0.20(D/H)\}cos2\theta + \{0.36 - 0.05(D/H)\}cos3\theta - \{0.14 - 0.05(D/H)\}cos4\theta \tag{2}$$

ring was also investigated utilizing Geometrically Nonlinear Analysis (GNA). The stress resultants developed in the IRS were calculated to be utilized as strength criteria This methodology has been used previously by Zeybek [9] and his coworkers [10] for the stability design of wind girders in open-top tanks. In the second stage, to discover the required stiffness of the IRS, the buckling of the shell was investigated by utilizing Linear Elastic Bifurcation Analysis (LBA). The buckling capacity of the storage tanks with an IRS at mid-height exposed to wind loads non-uniformly was examined considering internal suction. It should be noted that internal suction occurs under wind when the roof has not yet been installed. The relationship between the buckling resistance and the proposed CS-to- IRS stiffness ratio was studied through a comprehensive numerical parametric study. In addition, Geometrically Nonlinear Analysis including Imperfections (GNIA) was conducted to observe the impact of the imperfections on the buckling resistance of the CS by considering different imperfection amplitudes.

The structure of this paper consists of five main parts. The introduction is given in Section 1. The wind pressure variation on cylindrical shell structures is shown in Section 2. The derivation of the proposed CS-to-IRS stiffness criterion is presented in Section 3. Numerical studies employing LA, LBA, GNA and GNIA to develop the strength and stiffness requirements are provided in Section 4. Conclusions are given in Section 5.

where D = the diameter of the cylindrical tank shell, H = height of the cylindrical tank shell, $C_{p,e}$ = the normalized circumferential pressure distribution on the external side of the shell. It should be noted that the H/D ratio of 0.5 should be adopted for cylindrical structures with H/D ratios of <0.5.

The inner faces of the CS for open-top tank structures are also exposed to negative pressure because of the leeward suction. Thus, $C_{p,i} = -0.6$ is proposed as the coefficient of internal pressure irrespective of the tank size [37]. Recent studies [9,10] have reported that the effect of the negative pressure may be ignored in the flexural design of the wind girders. However, Chiang and Guzey [40] showed that the internal inward pressure exposed by wind load has a significant impact on the buckling capacity of the CS. Therefore, 2 design criteria should be fulfilled for the rings: stiffness and strength. In order to assure the stiffness, the ring should exhibit global shell buckling under wind load whereas to ensure the strength the ring should not yield under unsymmetrical forces due to wind loads [9,10].

3. Cylindrical shell-to-intermediate ring stiffener (CS-to-IRS) stiffness criterion

This section aims to obtain the relative stiffnesses of the CS and the IRS. Hence, the IRS and the CS were separately considered under nonuniform wind loads. The wind load in the radial direction ($q_r(\theta)$) can

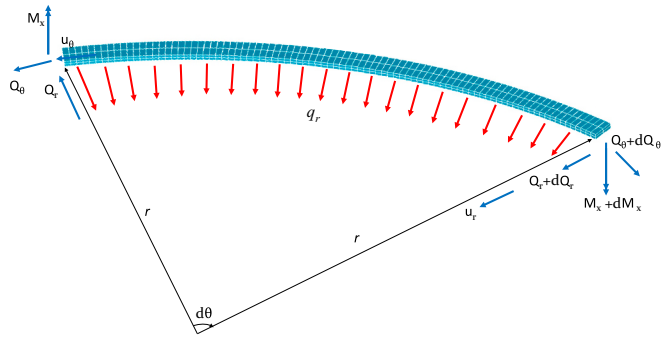

Fig. 4. Differential curved beam element and sign conventions.

be computed by taking into account the wind pressure shown in Eq. (1):

$$q_r(\theta) = C_m\, q\, h_{eff,m} cosm\theta \tag{2a}$$

where $h_{eff,m}$ is the tributary height.

The intermediate ring stiffener has to exhibit sufficient stiffness and strength to accurately fulfil its role. A reasonable criterion was developed taking into account the radial stiffnesses of the IRS and the CS. A proposed stiffness ratio of CS-to-IRS may be represented as (Ω) and given below in Eq. (3):

$$\Omega = \frac{K_{CS}}{K_{IRS}} = \frac{q_r(\theta)/u_{r,CS}}{q_r(\theta)/u_{r,IRS}} = \frac{u_{r,IRS}}{u_{r,CS}} \tag{3}$$

where K_{CS} = radial stiffness of the CS; and K_{IRS} = radial stiffness of the IRS; $u_{r,IRS}$ = radial displacement of the IRS; $u_{r,CS}$ = radial displacement of the CS.

Expressions for the closed-form solution are developed for the stiffness and stress resultants under radial non-uniform wind loads in the following subpart of the study.

3.1. Behaviour of an intermediate ring stiffener (IRS) under wind loading

Differential equations for curved beams derived from Vlasov [41,42] are employed to investigate the behaviour of the IRS. As shown in Fig. 4, the curved element is subjected to radial force (q_r). The resisting internal forces on the element are the shearing force in the radial direction (Q_r) and the normal force (Q_θ) in the circumferential direction; also the bending moment in the transverse (M_x). For the case where only radial wind loads (q_r) are acting, M_x can be found from Eq. (4):

$$M_x(\theta) = -\frac{C_m}{(m^2-1)} q\, h_{eff,m}\, r^2 cosm\theta \tag{4}$$

where r = radius of the IRS.

When an axisymmetric load ($m = 0$ or uniform internal pressure) is applied, no bending moment occurs about a tranverse axis ($M_x = 0$). Also, the first harmonic $m = 1$ can be ignored due to its negligible contribution to the responses of the ring [9,10]. For the higher harmonics (m ≥ 2), the following internal forces such as Q_r and Q_θ can also be determined for the IRS.

$$Q_r(\theta) = -\frac{m\, C_m}{(m^2-1)} q\, h_{eff,m}\, rsinm\theta \tag{5}$$

$$Q_\theta(\theta) = \frac{C_m}{(m^2-1)} q\, h_{eff,m}\, rcosm\theta \tag{6}$$

To identify the displacements in the IRS, the general force-deformation relationship of curved beams may be written relative to the centroidal axes:

$$Q_\theta = \frac{EA}{r}\left(\frac{du_\theta}{d\theta} - u_r\right) \tag{7}$$

$$M_x = \frac{EI_x}{r^2}\left(\frac{d^2u_r}{d\theta^2} + u_r\right) \tag{8}$$

where u_θ, u_r = displacements in the circumferential and radial directions respectively; I_x = the moment of inertia of the IRS about the transverse axis; A = cross sectional area of the IRS; E = elastic modulus.

The bending moment (M_x) in the transverse direction shown in Eq.

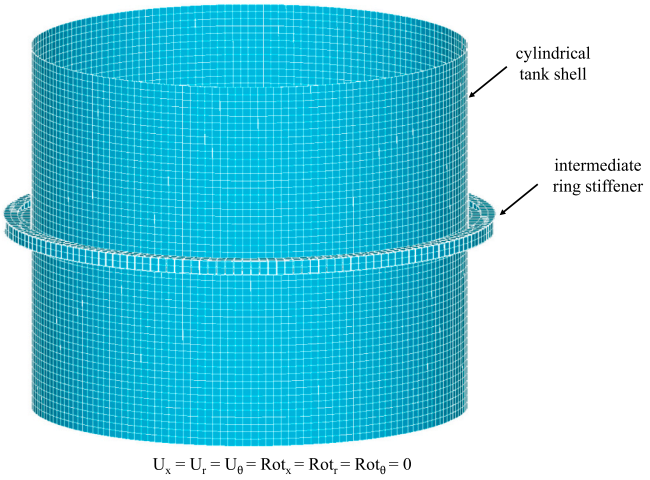

Fig. 6. Finite element mesh of the cylindrical steel tank with an intermediate ring stiffener (IRS) at mid-height (0.5H).

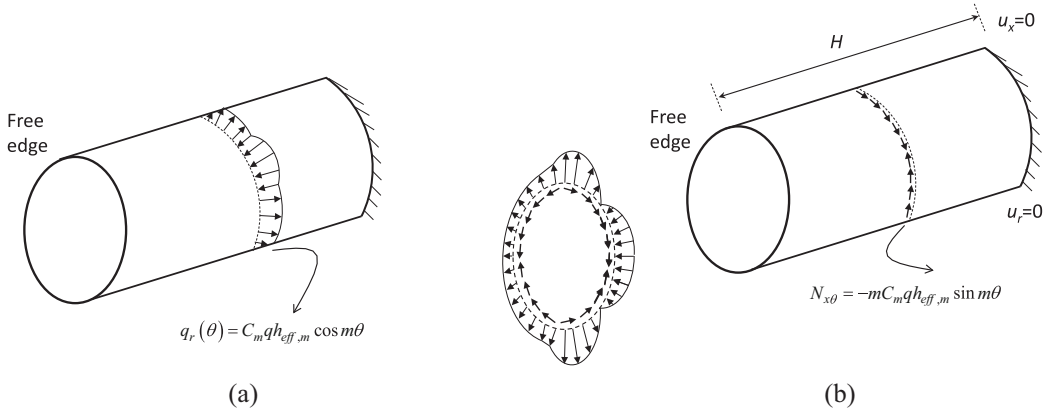

Fig. 5. Non- uniform line load in radial direction and shear load in circumferential direction.

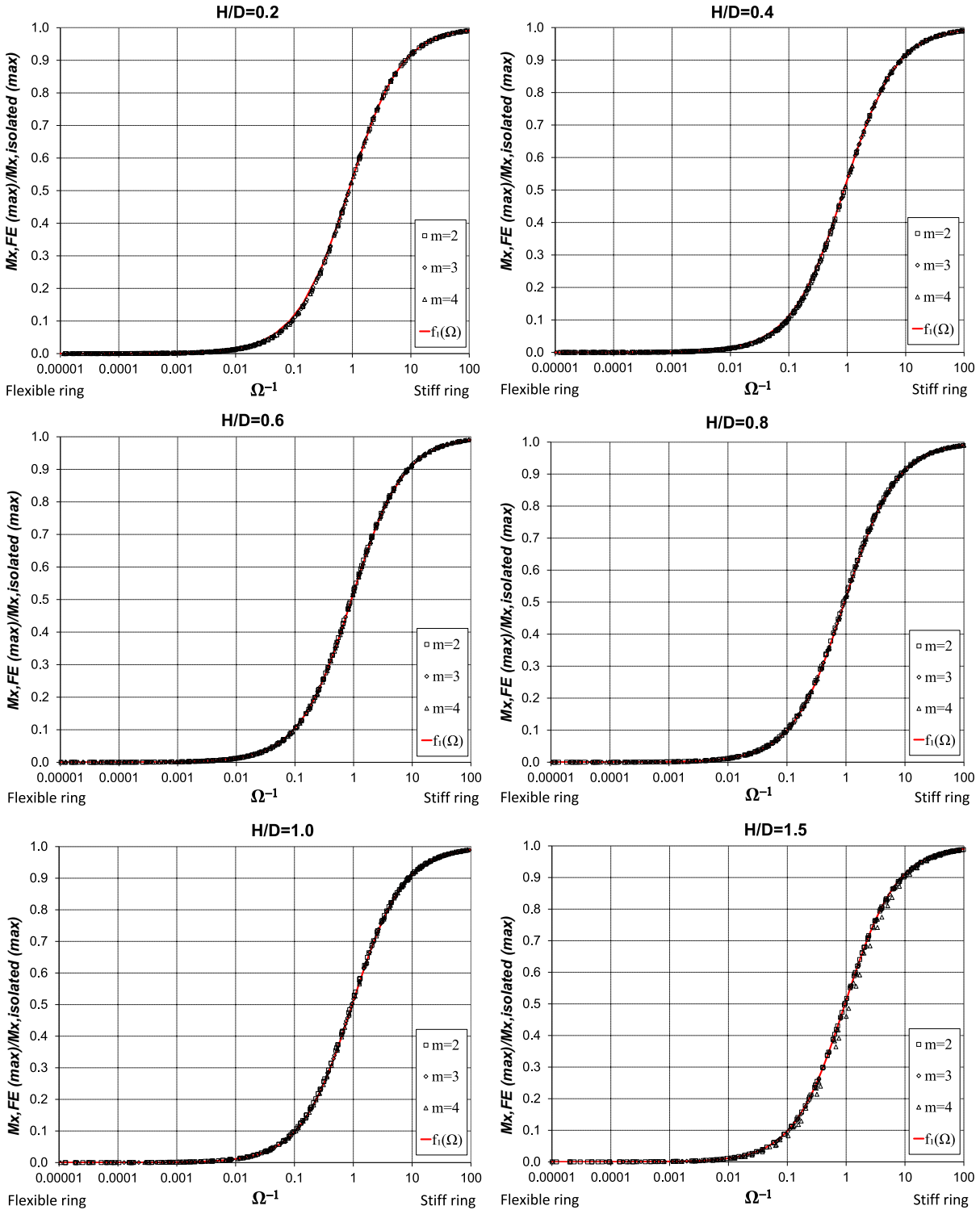

Fig. 7. Evaluation of the IRS and CS interaction for different height-to-diameter ratios.

Table 1
Constants for Eq. 14.

H/D	a_1	a_2
1.5	−0.000000001	0.98
1.0	−0.000001	0.97
0.8	−0.000001	0.96
0.6	−0.000001	0.94
0.4	−0.000001	0.91
0.2	−0.00004	0.90

(4) can be introduced into Eq. (8). The displacement in the radial (u_r) direction can be obtained by solving the differential equations to obtain:

$$u_r(\theta) = \frac{C_m}{(m^2-1)^2}\frac{q\, h_{eff,m}\, r^4}{EI_x} cos m\theta \tag{9}$$

The normal force in the circumferential direction and the radial direction displacement given by Eqs. (6 and 9) can be substituted in Eq. (7) and the following result for the displacement in the circumferential (u_θ) direction can be obtained:

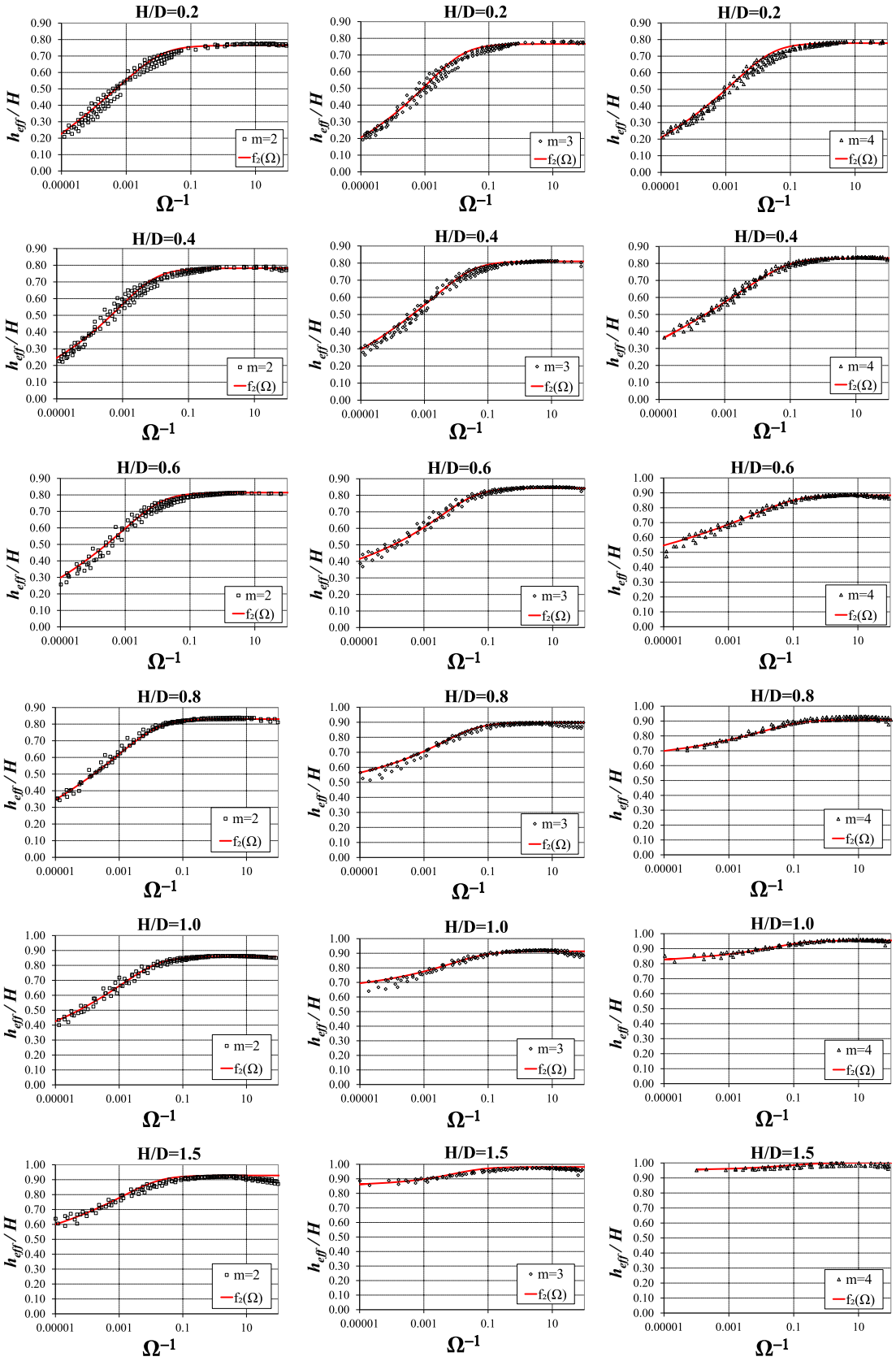

Fig. 8. Evaluation of the h_{eff} of the IRS for different height-to-diameter ratios.

Table 2
Constants for Eq. 15.

	$m = 2$				$m = 3$				$m = 4$			
H/D	a_3	a_4	a_5	a_6	a_3	a_4	a_5	a_6	a_3	a_4	a_5	a_6
1.5	0.33	0.98	82	0.112	0.85	0.36	32	0.29	0.95	0.07	3.2	0.26
1.0	0.08	1.3	85.7	0.115	0.62	0.47	19.1	0.16	0.8	0.22	7.12	0.18
0.8	−0.244	1.553	80.386	0.084	0.42	0.812	34.1	0.15	0.6	0.406	9.21	0.123
0.6	−0.226	1.659	107	0.1	0.21	1.076	40	0.144	0.175	0.832	10	0.07
0.4	−0.115	1.87	170	0.143	−0.276	1.47	40	0.082	−0.482	1.51	14.7	0.052
0.2	−0.91	2.167	100	0.056	−0.179	1.72	100	0.13	−0.29	1.58	50	0.1

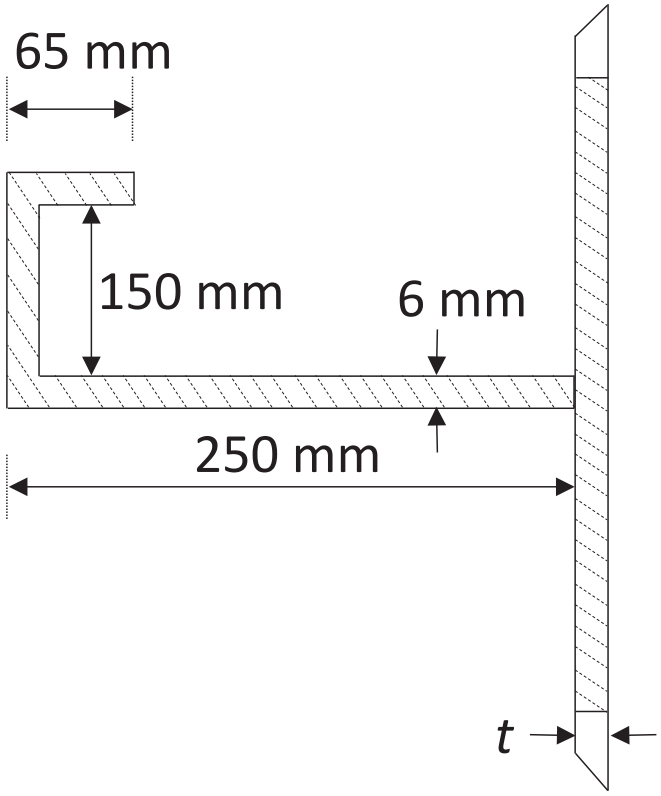

Fig. 9. Cross section of the detail for IRS.

$$u_\theta(\theta) = \frac{C_m}{m(m^2-1)^2}\,\frac{q\,h_{eff,m}\,r^2\left[(m^2-1)I_x + Ar^2\right]}{AEI_x}\,sinm\theta \tag{10}$$

3.2. Behaviour of a cylindrical shell (CS) under wind loading

Wind pressure is resisted by membrane shear in the CS ($m = 1$) which carries over the forces in transition to the base of the CS. Nevertheless, bending is created in both the IRS and the CS due to wind load which comprises higher harmonic loading components ($m \geq 2$). To obtain the stiffness of the CS, the same radial shear loading ($q_r(\theta)$) that was given in Eq. (2a) applied to the mid-height ($H/2$) of the CS given in Fig. 5.a is carried by a circular string [43]. The tangential shear loading ($N_{x\theta}$) at the mid-height of the CS (Fig. 5.b) may be converted from this non uniform load. The membrane theory of CS [44–47] was utilized taking into account the circular string to compute the radial stiffness of the CS under circumferential shear loading.

By introducing boundary conditions and proper loading which were given in Fig. 5, the radial displacements along the height of the CS can be computed as in Eq. (11):

$$u_r = m^2 C_m\, q\, h_{eff,m}\,\frac{x\left[12r^2(\nu+2) - 2x^2m^2 + 3Hm^2x\right]}{12Etr^2}\,cosm\theta \tag{11}$$

At the mid-height of the cylindrical shell ($x = H/2$), the displacement in the radial direction may be written as:

$$u_r = m^2 C_m\, q\, h_{eff,m}\,\frac{H\left[12r^2(\nu+2) + H^2m^2\right]}{24Etr^2}\,cosm\theta \tag{12}$$

The developed CS-to- IRS stiffness ratio (Ω) is calculated by substituting Eq. (9) and Eq. (12) into Eq. (3) as follows:

$$\Omega = \frac{1}{m^2(m^2-1)^2}\,\frac{24r^6t}{HI_x\left[12r^2(\nu+2) + m^2H^2\right]} \tag{13}$$

Eq. (13) reveals that proposed ratio (Ω) depends on the radius of the CS and the IRS (r), the thickness of the CS (t), the moment of inertia normal to the plane of the IRS (I_x), the Fourier harmonic (m) and the length of the CS (H).

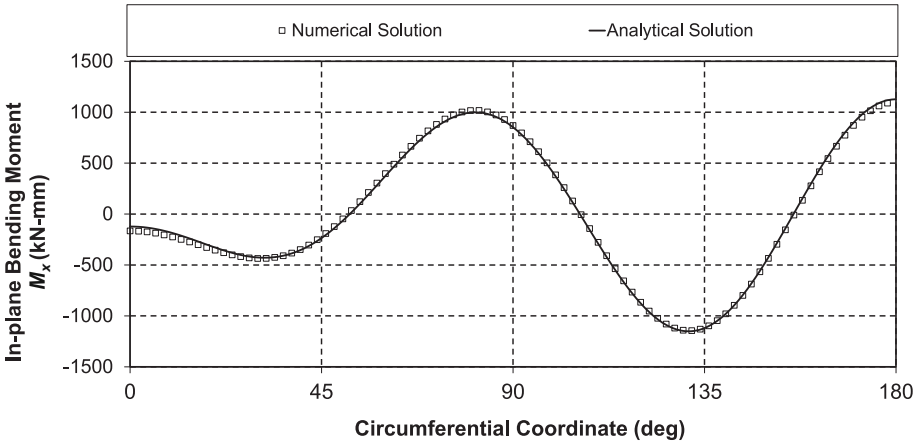

Fig. 10. Comparison of the proposed design solution with numerical findings for the IRS radial bending moment (M_x).

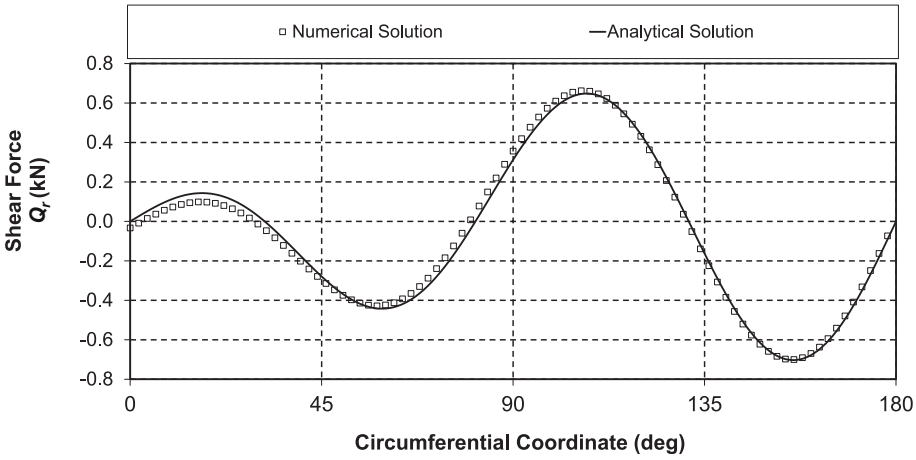

Fig. 11. Comparison of the proposed design solution with numerical findings for the IRS radial shear force (Q_r).

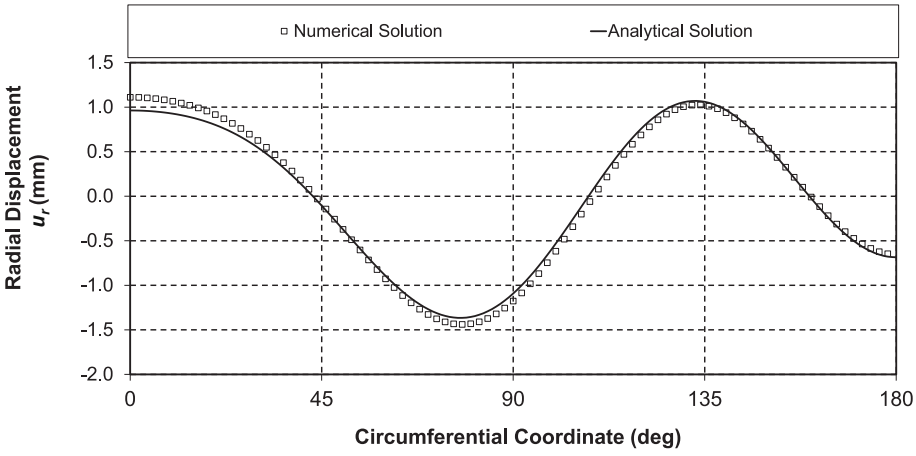

Fig. 12. Comparison of the proposed design solution with numerical findings for the IRS radial displacement (u_r).

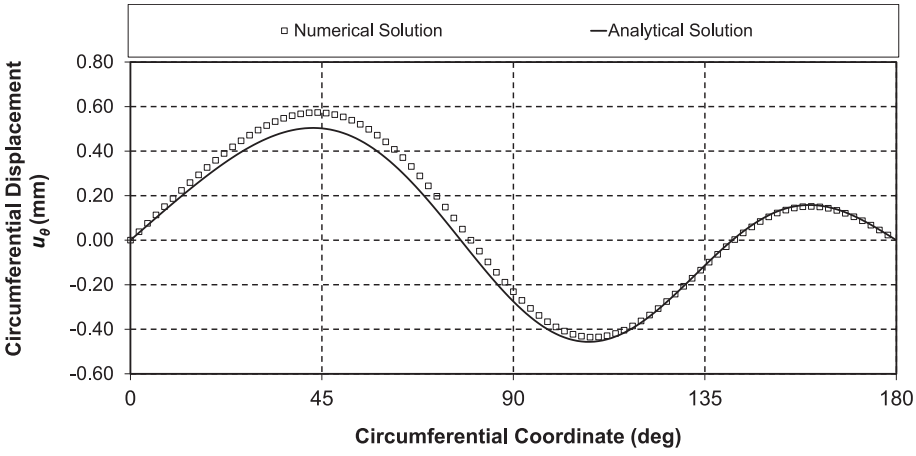

Fig. 13. Comparison of the proposed design solution with numerical findings for the IRS circumferential displacement (u_θ).

4. Numerical study

Numerical analyses were carried out mainly to propose criteria for the stability of cylindrical steel tanks with unrestrained upper edges (especially during the construction stage). Three dimensional FE analyses were conducted to determine the required stiffness and strength. The FE program ANSYS [48] was employed for the numerical analyses. A tank structure was created utilizing shell and beam elements as depicted in Fig. 6. Shell 63 elements were selected for the CS, whereas beam 4 elements were chosen for the IRS. All translations and rotations of shell bases were constrained to simulate the bottom edge of the CS [49]. A single IRS was installed to the models at mid-height ($H/2$) in order to enhance the buckling capacity. It should be noted the top of the cylindrical tank is free, so as to represent the unrestrained upper edge.

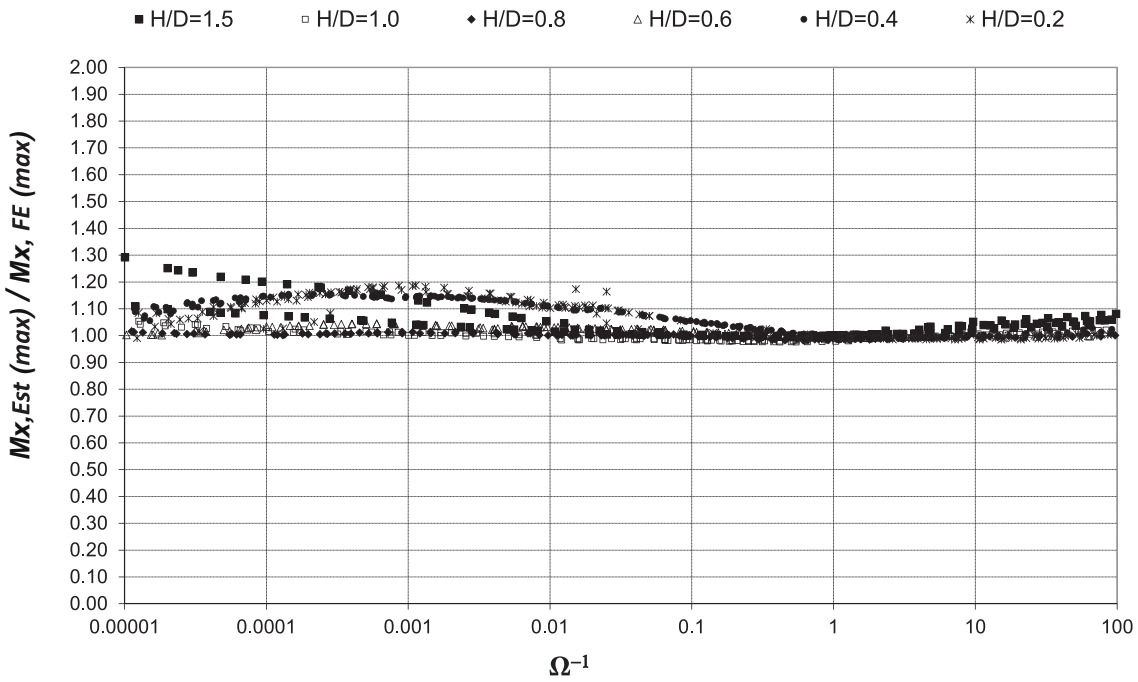

Fig. 14. Comparison of the proposed design solution with numerical findings for the in-plane bending moment in the IRS.

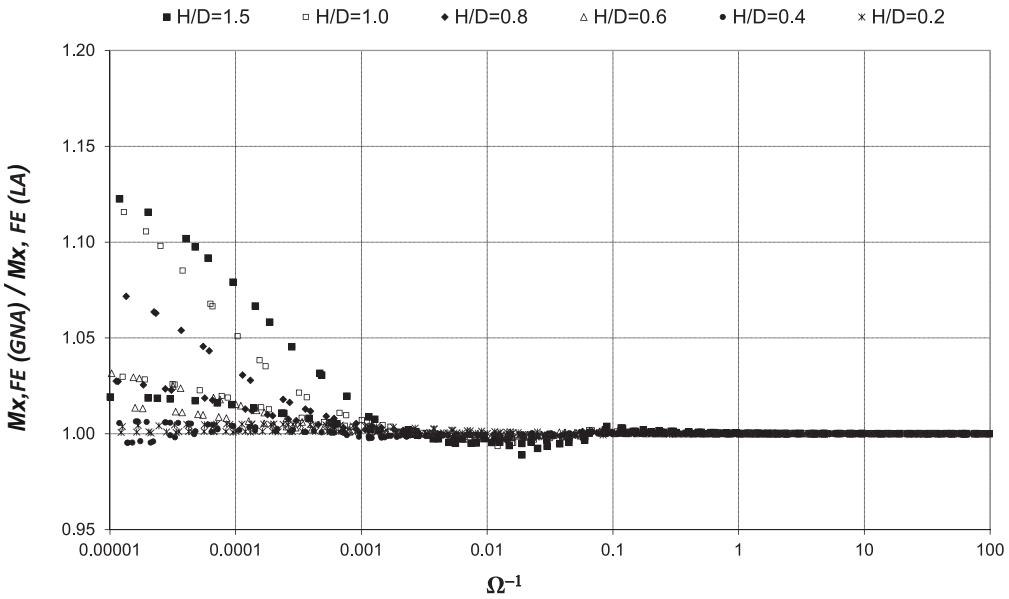

Fig. 15. Effects of geometrical nonlinearity on IRS bending moment.

The numerical work can be divided into two parts: (i) to examine the internal forces and moments in the IRS interacting with the CS, (ii) to identify the stiffness requirement of the IRS.

4.1. Stress resultants in intermediate ring stiffener (IRS) interacting with cylindrical tank shells

Two phased numerical parametric analyses were carried out in this first part. The first phase focused on the impact of the CS on the internal forces and moments of the IRS. The second phase concentrated on the h_{eff} for different loading conditions. According to a study conducted by Godoy [1], tanks are fabricated with rather short cantilever cylinders having radius-to-thickness ratios (r/t) ranging between 1000 and 2000 and height-to-diameter (H/D) ratios <1.0. Furthermore, Pantousa and Godoy [50] stated that most of the tanks studied in the literature have aspect ratios ranging between 0.25 and 1.0 [51]. Thus, H/D ratios between 0.2 and 1.5 were taken into consideration for simulations in the study. Different dimensions of annular plates were considered for the IRS in the parametric studies.

4.1.1. Cylindrical tank shell and intermediate ring stiffener interaction

The first phase investigates the impact of the CS in decreasing the internal forces and moments of the IRS. Since h_{eff} of the wind loading is initially unknown, the radial line load was implemented to the IRS [9,10]. It means that a variable loading along the circumference computed in Eq. Eq. (2a) was introduced rather than applying the wind pressure directly to the shell elements. 1.0 kPa × H wind load was selected for numerical models. Three harmonics of 2, 3, and 4 as

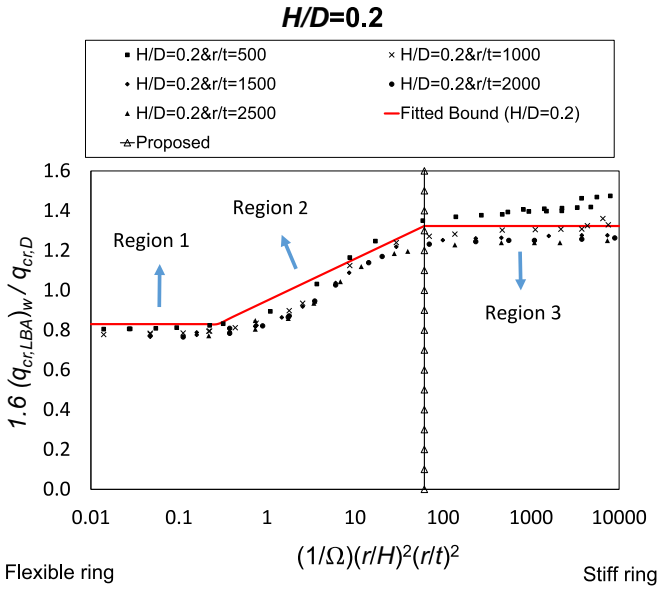

Fig. 16. Ratio of the buckling pressure with developed equation under wind loading for $H/D = 0.2$.

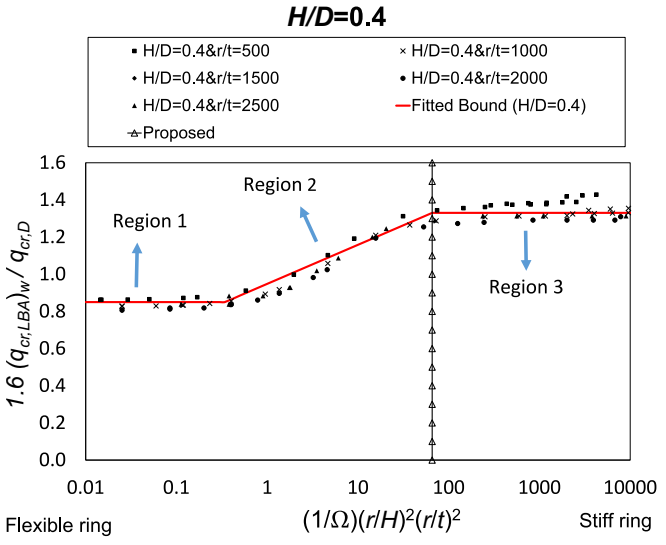

Fig. 17. Ratio of the buckling pressure with developed equation under wind loading for $H/D = 0.4$.

described in EN-1993-4-1 [37] were employed.

The maximum in-plane bending moment ($M_{x,FE}$ (max)) was obtained from the IRS data. Based on loadings with $m = 2$, 3, and 4, the reference term was computed utilizing Eq. (4). The values of $M_{x,FE}$ (max) were normalized by the values of $M_{x,isolated}$ (max) which is the reference in-plane bending moment. Normalized values for each analysis are plotted against Ω^{-1} as shown in Fig. 7. In this plot the normalized values for different H/D cases are presented separately. The results reveal that the stiffness ratio of CS-to-IRS (Ω) clearly mimics the trend of the data. Each of the data points for in-plane bending moment of the IRS fall within a rather narrow band. The data for different harmonics (m) obtained from each of the ratios *of H/D,* also follow the same trend. The analysis outcomes demonstrated that Ω can be employed for cylindrical steel tanks with an IRS to compute the changes in the response quantities because of the interaction between the IRS and the CS.

By applying curve-fitting to the data presented in Fig. 7, the following relationship between $M_{x,FE}$ and $M_{x,isolated}$ is developed:

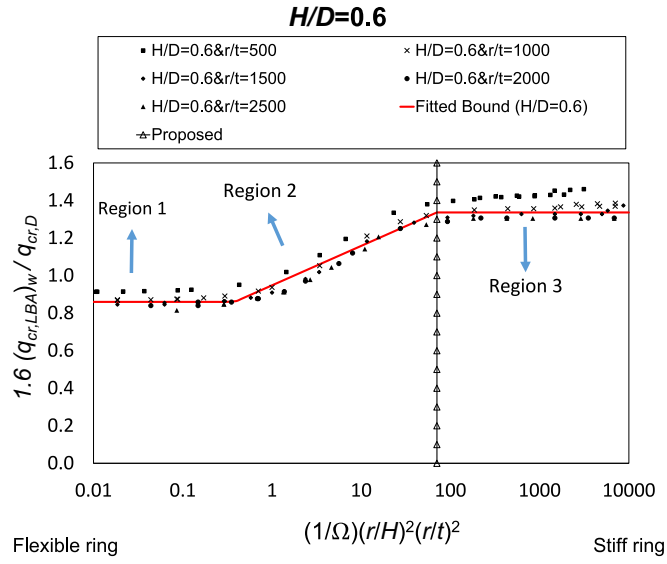

Fig. 18. Ratio of the buckling pressure with developed equation under wind loading for $H/D = 0.6$.

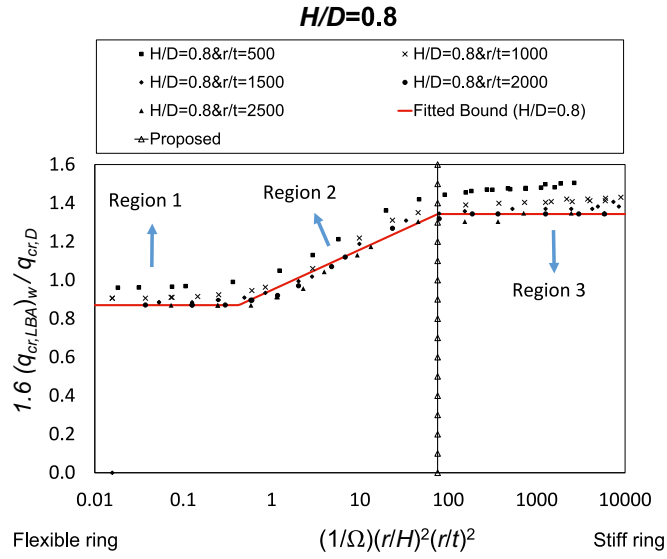

Fig. 19. Ratio of the buckling pressure with developed equation under wind loading for $H/D = 0.8$.

$$M_{x,FE}(\theta) = M_{x,isolated}(\theta)\, f_1(\Omega) \text{ and } f_1(\Omega) = a_1 + \frac{1}{(1+\Omega)^{a_2}} \quad (14)$$

where a_1 and a_2 were obtained by curve fitting and are shown in Table 1.

4.1.2. Tributary height for wind loading on the intermediate ring stiffener

In the second phase h_{eff} of wind loads was examined. In this phase, the same cases considered in the previous section were taken into account utilizing different loads. 1.0 kPa pressure changing depend on Eq. (1) was introduced to the CS instead of applying the loads directly to the IRS. A constant value was considered along the height, whereas the wind pressure was changing along the circumference. $M_{x,FE}$ (max) values were extracted from 2 circumstances and these were normalized to get h_{eff}. $M_{x,FE}$ (max) determined by using a changeable wind pressure on CS was normalized by $M_{x,FE}$ (max) determined by utilizing a variable loading on the IRS.

Ratios (h_{eff} /H) of $M_{x,FE}$ (max) were shown in Fig. 8 for different

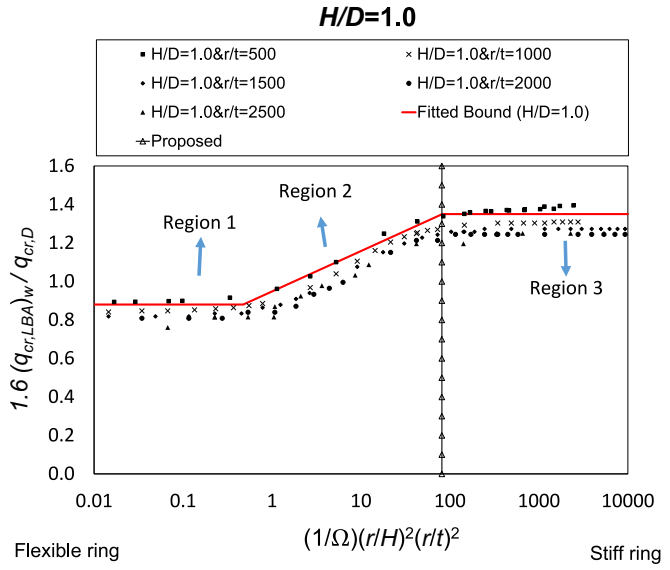

Fig. 20. Ratio of the buckling pressure with developed equation under wind loading for $H/D = 1.0$.

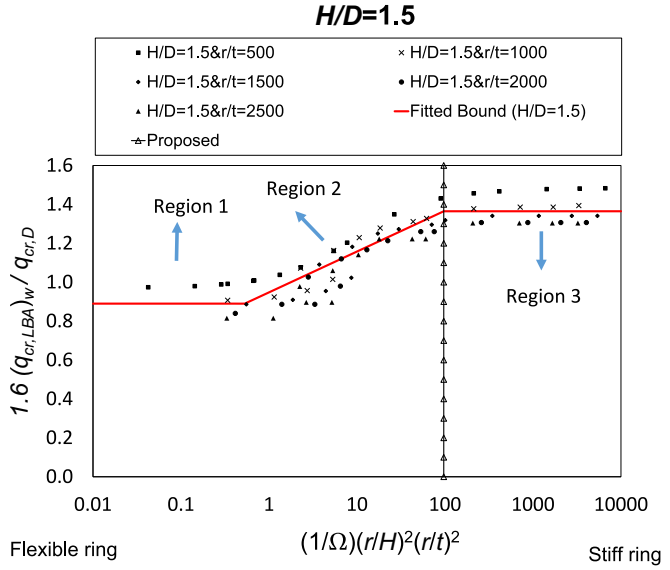

Fig. 21. Ratio of the buckling pressure with developed equation under wind loading for $H/D = 1.5$.

aspect ratios and harmonic numbers as a function of Ω^{-1}. The numerical outcomes indicate that a strong correlation is available between h_{eff}/H and Ω. h_{eff} increases as Ω^{-1} rises, but tends to saturate for $\Omega^{-1} > 1$, which represents cases with relatively stiff IRS. As shown in Fig. 8, the fitted bound shown in Eq. (15) was proposed to define the relationship between h_{eff}/H and Ω.

$$\frac{h_{eff,m}}{H} = f_2(\Omega) = a_3 + \frac{a_4}{(a_5 + \Omega)^{a_6}} \tag{15}$$

where a_3, a_4, a_5 and a_6 = constants that are depicted in Table 2.

4.1.3. Proposed expressions for stress resultants and displacements

Utilizing Eq. (4), Eq. (14) and Eq. (15), the variation of bending moment about the transverse axis ($M_{x,Est}(\theta)$) taking into account of each load term can be computed in Eq. (16):

$$M_{x,Est}(\theta) = -r^2 qH \sum_{m=2}^{N} \frac{C_m f_2(\Omega)}{(m^2-1)} f_1(\Omega)\, cos m\theta \tag{16}$$

The estimations for the radial shear force ($Q_{r,Est}(\theta)$), the radial displacement ($u_{r,Est}(\theta)$), and the circumferential displacement ($u_{\theta,Est}(\theta)$) can be computed from the following equations:

$$Q_{r,Est}(\theta) = -qrH \sum_{m=2}^{N} \frac{m\, C_m f_2(\Omega)}{(m^2-1)} f_1(\Omega) sin m\theta \tag{17}$$

$$u_{r,Est}(\theta) = \frac{qr^4}{EI_x} H \sum_{m=2}^{N} \frac{C_m f_2(\Omega)}{(m^2-1)^2} f_1(\Omega)\, cos m\theta \tag{18}$$

$$u_{\theta,Est}(\theta) = \frac{qr^2}{AEI_x} H \sum_{m=2}^{N} \frac{C_m \left[(m^2-1)I_x + Ar^2\right] f_2(\Omega)}{m(m^2-1)^2} f_1(\Omega)\, sin m\theta \tag{19}$$

4.1.4. Evaluation of the proposed design eqs

3D finite element analyses were utilized to assess the developed expressions. A specific case was chosen for the evaluation of the developed design equations. An open top CS with $r = 6000$ mm, $H = 12{,}000$ mm, and $t = 6$ mm was selected to evaluate the behaviour of the IRS. Instead of an annular plate cross-section, a IRS with a formed plate shown in Fig. 9 was considered for the verification of the developed expressions. 1.0 kPa nonuniform wind pressure was employed to the CS at the stagnation point. The coefficients defined in EN1993-4-1 [37] with all harmonics were taken for the circumferential variation of the pressure (Eq. (1)). Neverthless, vertical variation of the pressure was excluded since H/D is a small value.

The changes in the stress resultant and displacement values obtained from numerical analyses were compared with predictions from the proposed design equations (Eq. (16) - Eq. (19)). The calculated variations of M_x, Q_r, u_r and u_θ were depicted in Figs. 10, 11, 12 and 13 respectively. Harmonic terms of 0, 1, 2, 3 and 4 were utilized for the numerical part whereas harmonic terms of 2, 3 and 4 were used in the developed expressions. The evaluations showed that the proposed design equations offer acceptable estimates for the IRS in open top CS, with the maximum differences of 0.5%, 0.45%, 5.2% and 12.1% for the M_x, Q_r, u_r and u_θ respectively. As shown in Figs. 10, 11, 12 and 13, the effect of the 1st harmonic ($m = 1$) on the response quantities is very slight and thus did not lead to a noticable difference between the estimation of the proposed expressions and the findings of numerical simulations. However, greater differences were observed in the displacements, since the 1st harmonic stimulates a rigid body translation in the IRS. The goal of this study was to predict the moment M_x. Therefore,the 1st harmonic was omitted in this case since the 1st harmonic does not have an effect here. It should be indicated that maximum rate of the response quantities does not form at the stagnation point at all times. Therefore, the proposed design equations should not be evaluated at the stagnation point, and the maximum should be considered along the circumference.

The evaluation of the proposed design equations was enlarged by taking into account different height-to-diameter ratios which were utilized earlier to examine the response of an IRS interacting with the CS. $M_{x,FE}$ (max) was obtained from each finite element analysis and compared with the prediction of $M_{x,Est}$ (max) using Eq. (16). The ratios of $\Sigma M_{x,Est}$ (max) / $M_{x,FE}$ (max) were plotted against Ω^{-1} in Fig. 14 (considering the 2nd harmonic term). The average of the normalized moment values is 1.04, and the standard deviation of the values is 0.06.

The goal of the proposed expressions is to determine a strength criterion for the IRS taking LA into account. Furthermore, GNA was conducted to observe the impact of geometrical nonlinearity on the estimated $M_{x,FE}$ (max) in the IRS for the same H/D ratios. The comparison indicates that the normalized response quantity ($M_{x,\mathrm{FE}}$ (GNA)/ $M_{x,\mathrm{FE}}$ (LA)) differs by a maximum of 13% as shown in Fig. 15. According to the results, Ω has a strong effect on the discrepancy between the results.

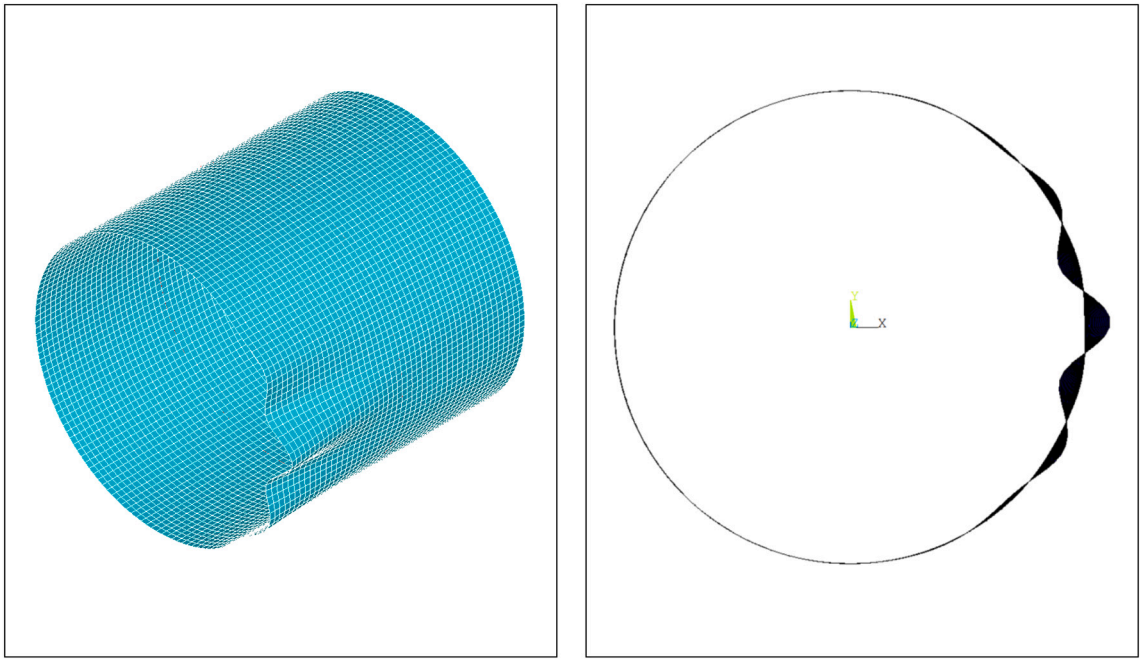

Fig. 22. First buckling mode of CS with an IRS.

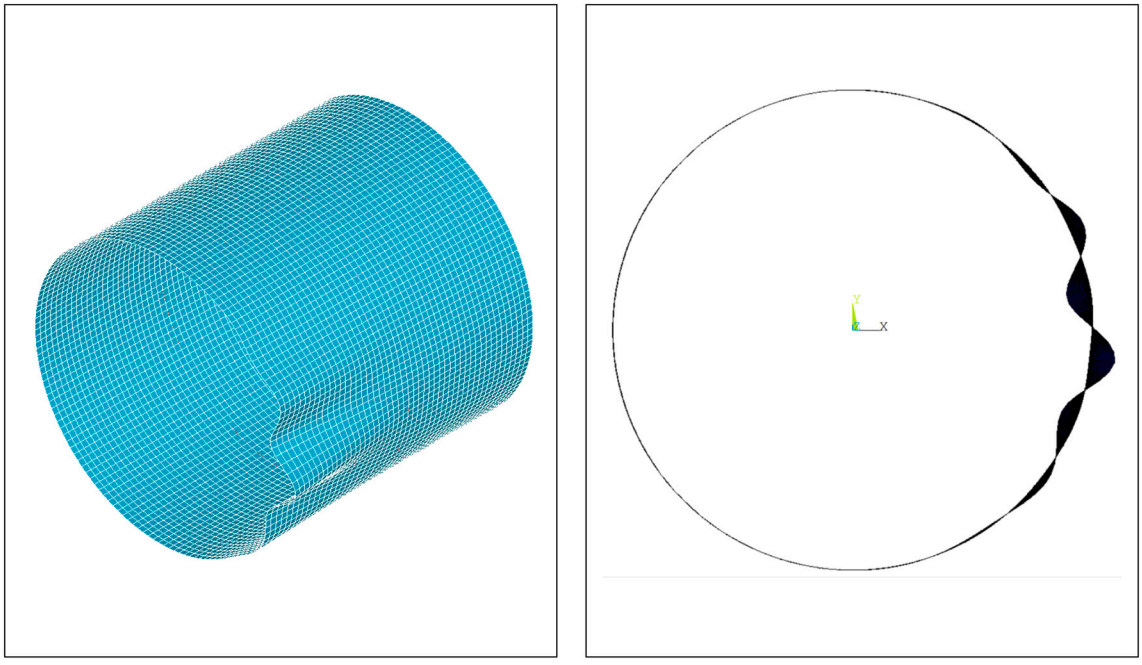

Fig. 23. Second buckling mode of CS with an IRS.

The normalized values ($M_{x,FE}$ (*GNA*)/ $M_{x,\ FE}$ (*LA*)) were seen to rise as Ω^{-1} decreases. In other words, when the ring is made more flexible, differences between $M_{x,FE}$ (*GNA*) and $M_{x,\ FE}$ (*LA*) are more pronounced.

4.2. Buckling of cylindrical steel tanks with an intermediate ring stiffener

The previous part has concentrated on the flexural design of the IRS. Solely accomplishing the strength criterion is not enough, since the IRS must also have sufficient stiffness to prevent buckling of the CS. Thus, a stiffness requirement is required to be developed for the IRS. In this part of the study, a detailed work is conducted to examine the buckling behaviour of the CS. For this purpose, the buckling capacity of the CS with an IRS exposed to non-uniform wind loading has been examined taking internal suction into account. First, LBA was carried out to identify the required stiffness of the IRS, then GNIA was conducted to determine the impact of geometrical imperfections on the buckling capacity of the CS with a single IRS.

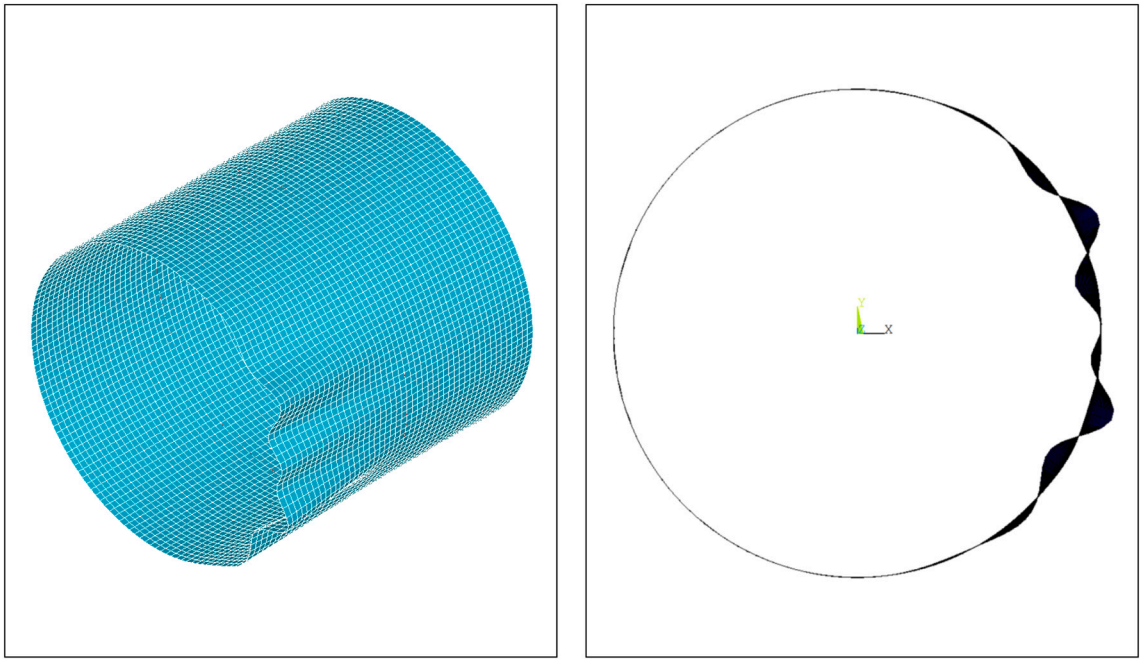

Fig. 24. Third buckling mode of CS with an IRS.

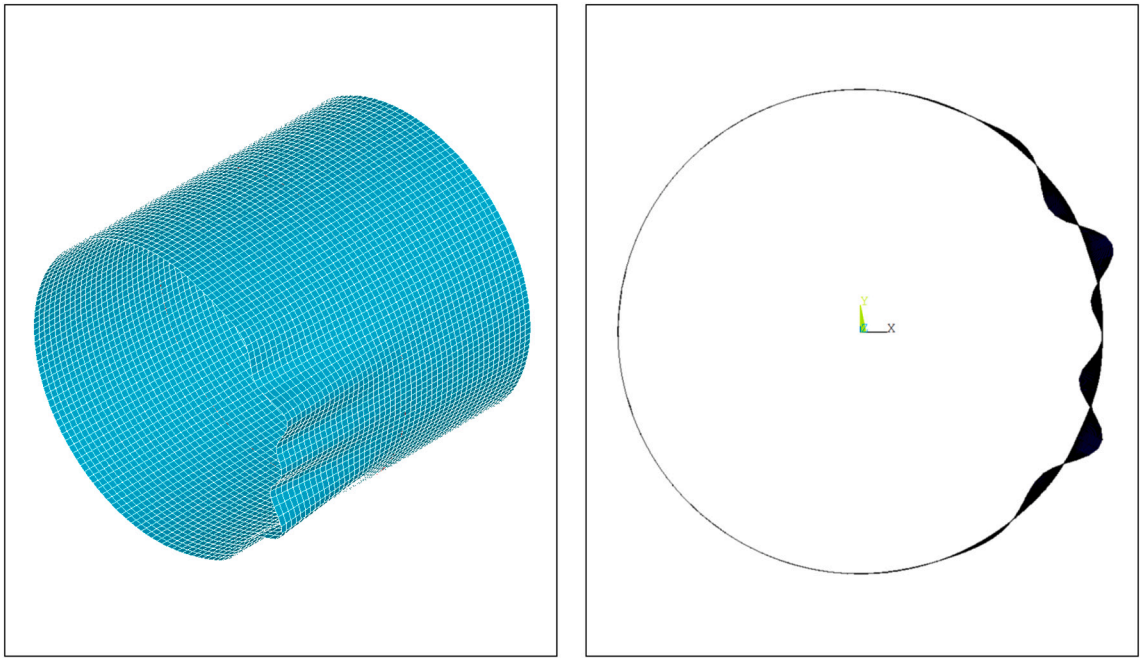

Fig. 25. Fourth buckling mode of CS with an IRS.

4.2.1. Linear buckling analysis (LBA) of cylindrical steel tanks with an intermediate ring stiffener

In this phase, the LBA of the CS with a single IRS was studied for the same ratios *of H/D* as in the previous phase. However, in this phase, *r/t* changes from 500 to 2500. A pressure of unity at the stagnation point of the shell surface was employed. The wind pressure profiles given by EN-1993-4-1 [37] were adopted. Negative inward pressure due to the leeward suction ($C_i = -0.6$) was also considered in the numerical models. The distribution of wind pressure was taken as constant along the height of the CS. LBA [52] was conducted to obtain the elastic critical buckling resistance, which is the first estimate of the elastic buckling strength. Considering the Donnell theory [53,54], a reference value for buckling capacity of uniform CS under uniform external pressure may be expressed as follows:

$$q_{cr,D} = 0.92E\left(\frac{t}{r}\right)^2\left(\frac{\sqrt{rt}}{H}\right) \tag{20}$$

The stagnation pressure at buckling $(q_{cr,LBA})_w$ from each finite

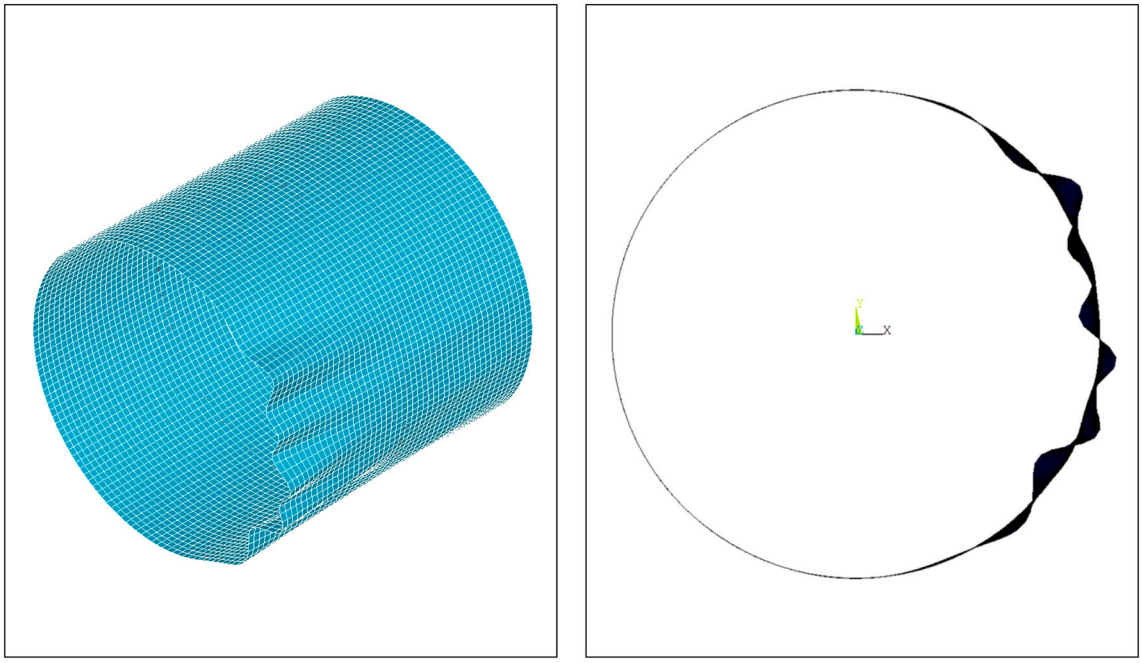

Fig. 26. Fifth buckling mode of CS with an IRS.

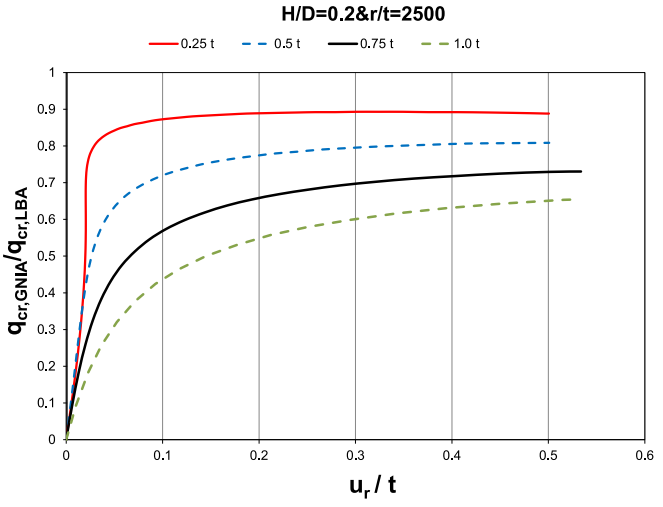

Fig. 27. Load – displacement curves obtained from GNIA results for H/D = 0.2&r/t = 2500.

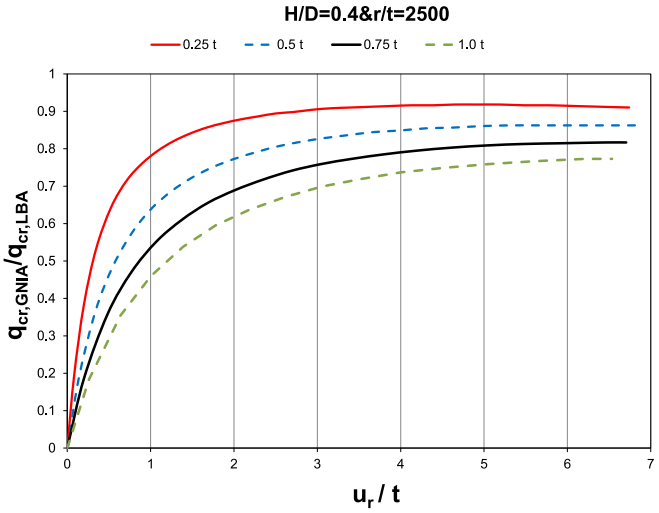

Fig. 28. Load – displacement curves obtained from GNIA results for H/D = 0.4&r/t = 2500.

element analysis was recorded. Then, 1.6 times $(q_{cr,LBA})_w$ was normalized by the reference buckling value $q_{cr,D}$. The value of 1.6 considers the influence of internal suction pressure. These ratios for wind loads are plotted in Figs. 16–21 as a function of inverse of the stiffness ratio of CS-to- IRS taking into account $m = 2$.

The decrease in the buckling resistance was determined in order to get the minimum necessary stiffness of the IRS. To achieve this aim, the relation between stiffness ratio of CS-to- IRS and normalized pressure in buckling may be represented for three areas as follows:

$$1.6\frac{\left(q_{cr,LBA}\right)_w}{q_{cr,D}} = 0.83 + 0.045\frac{H}{D} \text{ for region } 1 \tag{21}$$

$$1.6\frac{\left(q_{cr,LBA}\right)_w}{q_{cr,D}} = 0.948 + 0.21log\left[\left(\frac{1}{\Omega}\right)\left(\frac{r}{H}\right)^2\left(\frac{r}{t}\right)^2\right] \text{ for region } 2 \tag{22}$$

$$1.6\frac{\left(q_{cr,LBA}\right)_w}{q_{cr,D}} = 1.317 + 0.032\frac{H}{D} \text{ for region } 3 \tag{23}$$

By defining threshold limit values when the buckling resistance decreases, the required stiffness ratio of CS-to-IRS can be determined considering Eqs. (22–23):

$$\Omega = \frac{\left(\frac{r}{t}\right)^2\left(\frac{r}{H}\right)^2}{10^{\left(1.757+0.0762\frac{H}{r}\right)}} \tag{24}$$

The minimum I_x of IRS under wind loads is determined utilizing Eq. (13) and Eq. (24):

$$I_x = \frac{10^{\left(1.757+0.0762\frac{H}{r}\right)}r^2t^3H}{6\left(6.9r^2+H^2\right)} \tag{25}$$

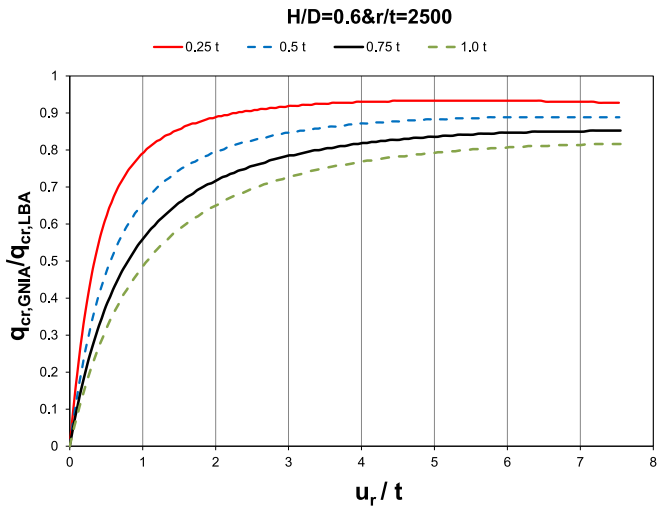

Fig. 29. Load – displacement curves obtained from GNIA results for H/D = 0.6&r/t = 2500.

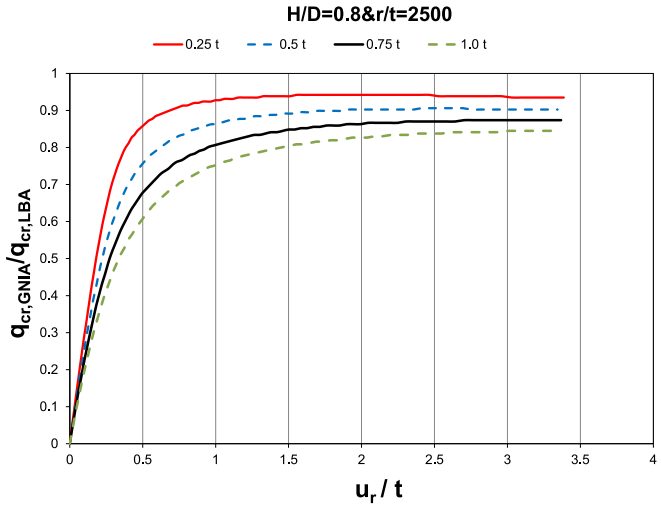

Fig. 30. Load – displacement curves obtained from GNIA results for H/D = 0.8&r/t = 2500.

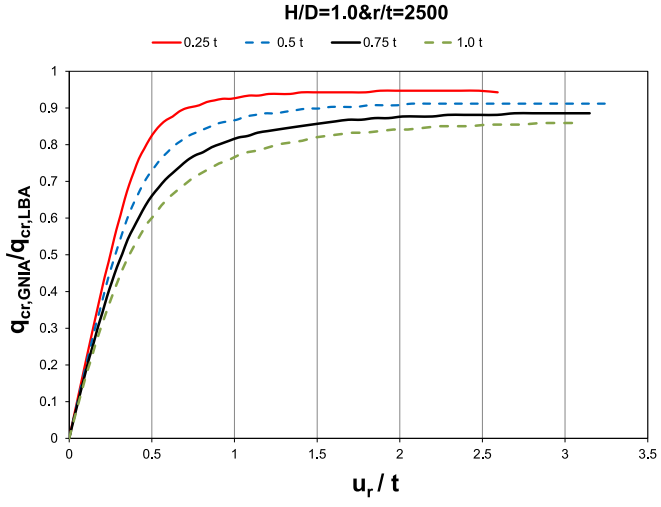

Fig. 31. Load – displacement curves obtained from GNIA results for H/D = 1.0&r/t = 2500.

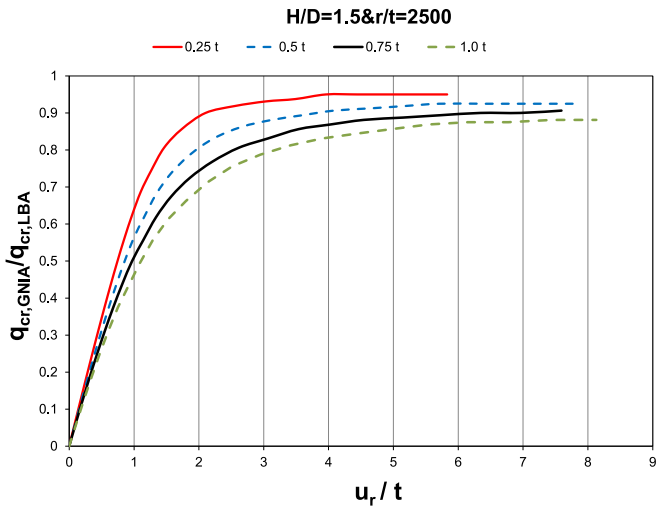

Fig. 32. Load – displacement curves obtained from GNIA results for H/D = 1.5&r/t = 2500.

Eq. (25) shows that proposed moment of inertia relies on only three properties: the radius of the CS and IRS (r), the height of the CS (H), and the thickness of the CS (t).

4.2.2. Geometrically nonlinear analysis including imperfections (GNIA) of cylindrical steel tanks with an intermediate ring stiffener

Imperfections significantly affect the capacity of thin CS structures. The developed stiffness requirement (moment of inertia) was evaluated by considering different imperfection amplitudes. The imperfections were utilized with the help of eigenmodes. First, considering a specific case, which is used in sub-part 4.1.4, five different buckling modes have been presented in Figs. 22 through 26. It should be noted that an annular plate wind girder was taken into account to satisy stiffness criteria. As shown here, for the specific case the 1st mode is symmetrical while the 2nd mode is unsymmetrical. The most detrimental shape of imperfection is the 1st mode which gives the lowest eigenvalue [1,55]. Thus, the first buckling mode was taken into account of geometrical imperfections on the buckling capacity of CS with an IRS in the study. Firstly, the eigenmode-affine pattern was obtained, then GNIA was carried out on the six different tank structures by considering imperfection amplitudes (Δ) of 0.25 t, 0.5 t, 0.75 t and 1.0 t. The radial displacement values (u_r) at the top along the stagnation meridian were recorded and normalized by the CS thickness (t). The ratios of the buckling pressure loads (q_{GNIA}/q_{LBA}) for six different diameter-to-height ratio cases are plotted against normalized values (u_r/t) in Figs. 27–32.

It is seen in Figs. 27–32 that, as the imperfection amplitude increases, the buckling strengths determined from GNIA (q_{GNIA}) deviate from LBA (q_{LBA}). In the 1.0 t imperfection amplitude, the $q_{cr,GNIA}/q_{cr,LBA}$ ratios extend to 0.88, 0.86, 0.84, 0.82, 0.77 and 0.65 for $H/D = 1.5$, $H/D = 1.0$, $H/D = 0.8$, $H/D = 0.6$, $H/D = 0.4$ and $H/D = 0.2$, respectively.

5. Conclusions

This paper has studied the effects of reinforcing steel tanks with stiffeners on wind buckling. The cylindrical shell part may be weak under environmental effects such as wind before the roof is installed. A combined numerical and analytical study was conducted to address this issue in the paper. In the study, a new stiffness ratio (Ω) of CS-to IRS was first derived to compute the ideal ring size in terms of both stiffness and strength. For the strength criteria, the tributary height and the effect of shell-girder interaction on the stress resultants were both investigated by making use of LA. In addition, GNA was conducted to investigate the effects of geometrical nonlinearity on the internal forces and moments. Furthermore, the IRS should exhibit enough stiffness to accomplish its

function accurately. To achieve these goals, the changes in the buckling resistance are investigated with the developed CS-to-IRS stiffness ratio when the CS is subjected to non-uniform wind load with internal suction. Depending on the Ω ratio, a novel stiffness criterion is proposed by taking into account the buckling strength of CS. In addition, GNIA was performed to examine the effect of the geometric imperfections on the buckling capacity of the CS with an IRS, taking different imperfection amplitudes into account. Based on this study, the following conclusions can be drawn:

- Using proposed expressions, the required strength and stiffness requirements of tank structures can be easily determined before a fixed roof is attached.
- Installing an intermediate ring stiffener increases the buckling capacity of the tank structures and it provides high stable behaviour during erection. In the case of inclusion of a stiff IRS at mid-height of CS, an increase in the buckling capacity of >50% was observed.
- For a safe design against shell buckling, the ideal IRS size can be identified using developed equations without the need for an onerous finite element analysis.
- Geometric nonlinearity and geometric imperfections used the eigenmode-affine imperfection adversely affect buckling strength of the cylindrical shell structures. The analysis results also indicate that the reduction in the amount of strength increases as the height-to-diameter ratio decreases.

The results of our study show that tank structures have low strength and stiffness before they are completed and their roofs are installed. It is recommended that strength and stiffness criteria must be met to ensure stable behaviour during construction phases.

CRediT authorship contribution statement

Özer Zeybek: Writing – original draft, Writing – review & editing, Investigation, Conceptualization, Methodology. **Yasin Onuralp Özkılıç:** Writing – original draft, Writing – review & editing.

Declaration of Competing Interest

The authors declare that they have no known competing financial interests or personal relationships that could have appeared to influence the work reported in this paper.

Data availability

No data was used for the research described in the article.

Acknowledgements

The Authors would like to thank Mr. Oscar Enrique Morillo Luzardo for providing Fig. 1. More deteails can be found here [56].

References

[1] L.A. Godoy, Buckling of vertical oil storage steel tanks: review of static buckling studies, Thin-Walled Struct. 103 (2016) 1–21.
[2] H. Saal, W. Schrufer, Stability of wind-loaded shells of cylindrical tanks with unrestrained upper edge, in: J.F. Jullien (Ed.), Buckling of Shell Structures, on Land, in the Sea and in the Air, Elsevier Applied Science, London, 1991, pp. 223–232.
[3] P. Ansourian, On the buckling analysis and design of silos and tanks, J. Constr. Steel Res. 23 (1992) 273–294.
[4] R.K. Noon, Forensic Engineering Investigation, CRC Press, Boca Raton, FL, 2001.
[5] S. Borgersen, S. Yazdani, Finite element analysis of wind induced buckling of steel tank, in: N. Ghafoori (Ed.), Challenges, CRC Press, Boca Raton FL, Opportunities and Solutions in Structural Engineering and Construction, 2010, pp. 157–160.
[6] R.C. Jaca, L.A. Godoy, Wind buckling of metal tanks during their construction, Thin-Walled Struct. 48 (2010) 453–459.
[7] F. Bu, C. Qian, A rational design approach of intermediate wind girders on large storage tanks, Thin-Walled Struct. 92 (2015) 76–81.
[8] EN 14015:2004, Specification for the Design and Manufacture of Site Built, Vertical, Cylindrical, Flat-Bottomed, above Ground, Welded, Steel Tanks for the Storage of Liquids at Ambient Temperature and Above, CEN, Brussels, 2005.
[9] Ö. Zeybek, C. Topkaya, J.M. Rotter, Stress resultants for wind girders in open-top cylindrical steel tanks, Eng. Struct. 196 (2019), 109347.
[10] Ö. Zeybek, The stability of anchored cylindrical steel tanks with a secondary stiffening ring, Int. J. Press. Vessel. Pip. 198 (2022), 104661.
[11] F.J. Maher, Wind loads in dome-cylinder and dome-cone shapes, ASCE J. Struct. Div. 92 (5) (1966) 79–96.
[12] A. Raeesi, H. Ghaednia, J. Zohrehheydariha, S. Das, Failure analysis of steel silos subject to wind load, Eng. Fail. Anal. 79 (2017) 749–761.
[13] S. Maleki, Alireza Moazezi Mehretehran, 3D wind buckling analysis of long steel corrugated silos with vertical stiffeners, Eng. Fail. Anal. 90 (2018) 156–167.
[14] A.M. Mehretehran, S. Maleki, Seismic response and failure modes of steel silos with isotropic stepped walls: the effect of vertical component of ground motion and comparison of buckling resistances under seismic actions with those under wind or discharge loads, Eng. Fail. Anal. 120 (2021), 105100.
[15] F. Resinger, R. Greiner, Buckling of wind-loaded cylindrical shells - application to unstiffened and ring-stiffened tanks, in: E. Ramm (Ed.), Buckling of Shells, Springer-Verlag, Berlin, 1982, pp. 305–332.
[16] D.M. Purdy, F.J. Maher, D. Frederick, Model studies of wind loads on flat-top cylinders, ASCE J. Struct. Div. 93 (1967) 379–398.
[17] M. Esslinger, S. Ahmed, H. Schroeder, Stationary wind loads of open-topped and roof-topped cylindrical silos (in German), in: Der Stahlbau, 1971, pp. 1–8.
[18] P.A. MacDonald, K.C.S. Kwok, J.D. Holmes, Wind loads on circular storage bins, silos and tanks: I. point pressure measurements on isolated structures, J. Wind Eng. Ind. Aerodyn. 31 (1988) 165–188.
[19] P.A. MacDonald, J.D. Holmes, K.C.S. Kwok, Wind loads on circular storage bins, silos and tanks: II. Effect of grouping, J. Wind Eng. Ind. Aerodyn. 34 (1990) 77–95.
[20] P.A. Macdonald, J.D. Holmes, K.C.S. Kwok, Wind loads on circular storage bins, silos and tanks. III. Fluctuating and peak pressure distributions, J. Wind Eng. Ind. Aerodyn. 34 (3) (1990) 319–337.
[21] H. Pasley, C. Clark, Computational fluid dynamics study of flow around floating-roof oil storage tanks, J. Wind Eng. Ind. Aerodyn. 86 (1) (2000) 37–54.
[22] G. Portela, L.A. Godoy, Wind pressures and buckling of cylindrical steel tanks with a conical roof, J. Constr. Steel Res. 61 (6) (2005) 786–807.
[23] Y. Uematsu, C. Koo, J. Yasunaga, Design wind force coefficients for open-topped oil storage tanks focusing on the wind-induced buckling, J. Wind Eng. Ind. Aerodyn. 130 (2014) 16–29.
[24] Y. Uematsu, T. Yamaguchi, J. Yasunaga, Effects of wind girders on the buckling of open-topped storage tanks under quasi-static wind loading, Thin-Walled Struct. 124 (2018) 1–12.
[25] J. Yasunaga, Y. Uematsu, Dynamic buckling of cylindrical storage tanks under fluctuating wind loading, Thin-Walled Struct. 150 (2020), 106677.
[26] F. Bu, C. Qian, On the rational Design of the top Wind Girder of large storage tanks, Thin-Walled Struct. 99 (2016) 91–96.
[27] A.R. Shokrzadeh, M.R. Sohrabi, Buckling of ground based steel tanks subjected to wind and vacuum pressures considering uniform internal and external corrosion, Thin-Walled Struct. 108 (2016) 333–350.
[28] E. Azzuni, S. Guzey, Stability of open top cylindrical steel storage tanks: design of top wind girder, ASME J. Press. Vessel Technol. 139 (2017) 312–322.
[29] T. Sun, E. Azzuni, S. Guzey, Stability of open-topped storage tanks with top stiffener and one intermediate stiffener subject to wind loading, ASME J. Press. Vessel Technol. 140 (1) (2018), 011204.
[30] Q.S. Cao, Y. Zhao, R. Zhang, Wind induced buckling of large circular steel silos with various slenderness, Thin-Walled Struct. 130 (2018) 101–113.
[31] J. Pan, S. Liang, Buckling analysis of open-topped steel tanks under external pressure, SN Appl. Sci. 2 (2020) 535.
[32] R. Greiner, Cylindrical shells: wind loading. Chapter 17, in: C.J. Brown, L. Nilssen (Eds.), Silos, EFN Spon, London, 1998, pp. 378–399.
[33] J.M. Rotter, Membrane theory of shells for bins and silos, in: Transactions of Mechanical Engineering, Institution of Engineers, Australia Vol. ME12, 1987, pp. 135–147. No.3 September.
[34] R.F. Rish, Forces in cylindrical chimneys due to wind, Proc. Inst. Civ. Eng. 36 (1967) 791–803.
[35] D. Briassoulis, D.A. Pecknold, Behavior of empty steel grain silos under wind loading: part 1: the stiffened cylindrical shell, Eng. Struct. 8 (4) (1986) 260–275.
[36] ACI-ASCE Committee 334, Reinforced Concrete Cooling Tower Shells-Practice and Commentary, ACI 334, 2R, 91, American Concrete Institute, New York, 1991.
[37] EN 1993-4-1, Eurocode 3: Design of steel structures, Part 4.1: Silos, Eurocode 3 Part 4.1, CEN, Brussels, 2007.
[38] M. Pircher, W. Guggenberger, R. Greiner, Stresses in elastically supported cylindrical shells under wind load and foundation settlement, Adv. Struct. Eng. 4 (3) (2001) 159–167.
[39] P.L. Gould, W.B. Kratzig, Cooling tower structures, in: W. Chen (Ed.), Handbook of Structural Engineering, CRC Press Inc, Boca Raton, FL, 1998, pp. 473–504.
[40] Y. Chiang, S. Guzey, Influence of internal inward pressure on stability of open-top aboveground steel tanks subjected to wind loading, ASME. J. Press. Vessel Technol. 141 (3) (2019), 031204.
[41] V.Z. Vlasov, Thin-Walled Elastic Beams, National Science Foundation, Washington, D.C., 1961.
[42] C.P. Heins, Bending and Torsional Design in Structural Members, Lexington Books, Lexington, Massachusetts, 1975.
[43] C.R. Calladine, Theory of Shell Structures, Cambridge University Press, U.K, 1983.

[44] S.P. Timoshenko, S. Woinowsky-Krieger, Theory of Plates and Shells, McGraw-Hill, New York, 1959.
[45] W. Flügge, Stresses in Shells, Springer-Verlag, Berlin, 1973.
[46] P. Seide, Small Elastic Deformations of Thin Elastic Shells, Noordhoff, Leyden, Holland, 1975.
[47] E. Ventsel, T. Krauthammer, *Thin Plates and Shells: Theory, Analysis* and Applications, Marcel Dekker, NY, 2001.
[48] ANSYS, Version 12.1 On-Line User's Manual, 2010.
[49] Y. Zhao, Y. Lin, Buckling of cylindrical open-topped steel tanks under wind load, Thin-Walled Struct. 79 (2014) 83–94.
[50] D. Pantousa, L.A. Godoy, On the mechanics of thermal buckling of oil storage tanks, Thin-Walled Struct. 145 (2019), 106432.
[51] H. Bohra, S. Guzey, Fitness-for-service of open-top storage tanks subjected to differential settlement, Eng. Struct. 225 (2020), 111277.
[52] EN 1993-1-6, Eurocode 3: Part 1.6: Strength and Stability of Shell Structures. CEN, Brussels, 2007.
[53] L.H. Donnell, Effect of imperfections on buckling of thin cylinders under external pressure, J. Appl. Mech., ASME 23 (4) (1956) 569–575.
[54] L.H. Donnell, Effect of imperfections on buckling of thin cylinders with fixed edges under external pressure, proc. 3rd U.S, Nat. Conger. Appl. Mech (1958) 305–311.
[55] Ö. Zeybek, C. Topkaya, Stiffness requirements for wind girders in open-top cylindrical steel tanks, Thin-Walled Struct. 176 (2022), 109353.
[56] O.E.M. Luzardo, The Tank was Deformed/Bent during its Erection due to the Action of the Wind — Why?. https://www.linkedin.com/pulse/tank-deformedbent-during-its-erection-due-action-wind-oscar-enrique/, 2020.